

Dynamics of longitudinal magnetization in transverse-field quantum Ising model: from symmetry-breaking gap to Kibble-Zurek mechanism

Michał Białończyk and Bogdan Damski

Jagiellonian University, Marian Smoluchowski Institute of Physics, Łojasiewicza 11, 30-348 Kraków, Poland
(01/10/2019)

We show that the symmetry-breaking gap of the quantum Ising model in the transverse field can be extracted from free evolution of the longitudinal magnetization taking place after a gradual quench of the magnetic field. We perform for this purpose numerical simulations of both periodic and open Ising chains. We also study the condition for adiabaticity of evolution of the longitudinal magnetization finding excellent agreement between our simulations and the prediction based on the Kibble-Zurek theory of non-equilibrium phase transitions. Our results should be relevant for ongoing cold atom and ion experiments targeting either equilibrium or dynamical aspects of quantum phase transitions.

I. INTRODUCTION

Quantum phase transitions take place when tiny changes of the external parameter, such as the magnetic field in spin models or the lattice height in cold atom setups, can induce radical changes in ground state properties of the system [1–4]. This can happen when the system is near the critical point separating its phases.

One of the typical features associated with quantum phase transitions is the symmetry-breaking phenomenon, where one of the phases of the thermodynamically-large system has degenerate ground states, which do not respect the symmetry of the Hamiltonian. Such a degeneracy is typically lifted in finite systems, where a small energy gap between lowest-energy eigenstates of the Hamiltonian is present. Rapid disappearance of this gap with increase of the system size signals the onset of the symmetry-breaking phenomenon that is fundamentally important for understanding of both equilibrium and non-equilibrium phase transitions. It is thus very interesting to address the question how one can access the symmetry-breaking gap in real systems to observe emergence of such a compelling phenomenon.

We make a step forward in this direction by providing an explicit scheme for studies of the symmetry-breaking gap in the quantum Ising model in the transverse field. We expect that our approach can be generalized to other, not necessarily exactly solvable systems, which can be experimentally studied in cold atom and ion simulators of various condensed matter models [4, 5]. In fact, while pursuing this work, we have come across a recent preprint discussing experimental studies of the symmetry-breaking gap in a cold atom cloud [6]. We will first discuss our results and then compare the two approaches in Sec. V.

To explain the idea behind our proposal, we introduce the quantum Ising model in the transverse magnetic field g , whose Hamiltonian in the periodic chain can be written as [7]

$$H(g) = - \sum_{i=1}^N (\sigma_i^x \sigma_{i+1}^x + g \sigma_i^z), \quad (1)$$

$$\sigma_{N+1}^x = \sigma_1^x,$$

where $\sigma_j^{x,y,z}$ is the Pauli matrix acting on the j -th spin, N is the number of spins, and $g \geq 0$ is assumed thought this work. Such a model has two phases: the ferromagnetic phase for $0 \leq g < 1$ and the paramagnetic phase for $g > 1$. The breaking of the \mathbb{Z}_2 symmetry of this model, associated with the $\sigma_j^x \rightarrow -\sigma_j^x$ symmetry of the Hamiltonian, can be easily explained at $g = 0$, when the two

ground states have all spins aligned in the $\pm x$ direction

$$|\rightarrow\rightarrow\rightarrow\cdots\rangle, |\leftarrow\leftarrow\leftarrow\cdots\rangle. \quad (2)$$

Then an arbitrarily small perturbation along the x direction, say $-h \sum_i \sigma_i^x$ with $h \rightarrow 0^+$, makes $|\rightarrow\rightarrow\rightarrow\cdots\rangle$ the ground state of the system breaking the spin-flip symmetry supported by the Hamiltonian. Importantly, degeneracy of the ground state, in thermodynamically-large systems, persists in the whole ferromagnetic phase.

The idea that we have is that one can initially set $g = 0$ and prepare the system in one of the states given in (2), say

$$|\psi(t=0)\rangle = |\rightarrow\rightarrow\rightarrow\cdots\rangle. \quad (3)$$

We propose then to evolve the system according to the following protocol

$$g(t) = \begin{cases} g_f + t/\tau_Q & \text{for } -g_f\tau_Q \leq t \leq 0 \\ g_f & \text{for } t > 0 \end{cases} \quad (4)$$

with τ_Q controlling the rate of driving the system to the magnetic field g_f , where free evolution begins. To place our research in a wider context, we mention that different aspects of dynamics of the quantum Ising model–induced by a gradual, i.e., $\tau_Q \neq 0$, change of the magnetic field–were studied in [8–24].

The natural observable for studies of the symmetry-breaking gap is the longitudinal magnetization

$$M_x = \langle \sigma_i^x \rangle, \quad (5)$$

where the choice of the site index i is arbitrary in a periodic chain. Such an observable is sensitive to the way in which the symmetry is broken. Indeed, it is well-known that

$$-M_x^{eq} \leq M_x \leq M_x^{eq}, \quad (6)$$

where in the thermodynamically-large system [25]

$$M_x^{eq} = \begin{cases} (1 - g^2)^{1/8} & \text{for } 0 \leq g \leq 1 \\ 0 & \text{for } g > 1 \end{cases}. \quad (7)$$

M_x^{eq} will be called the equilibrium longitudinal magnetization and it will be computed not only in the $N \rightarrow \infty$ limit. This is illustrated in Fig. 1, where we see that M_x^{eq} is analytic in finite systems. In such systems, the drop of the longitudinal magnetization is not as steep as in (7) on the ferromagnetic side. On the paramagnetic side, non-zero value of M_x^{eq} appears–see (26) and discussion around it.

The question now is how the symmetry-breaking gap can be extracted from dynamics of the longitudinal magnetization. To explain that, we first note that the expectation value of the σ_j^x operator vanishes in all eigenstates of Hamiltonian (1) for $g > 0$. This can be proved with Wick’s theorem in the fermionic representation of the Ising model, which we briefly introduce in Sec. III. Result (7) is obtained by evaluation of (5) in a proper superposition of two eigenstates of the Hamiltonian followed by the $N \rightarrow \infty$ limit. In fact, deceptively simple-looking initial state (3) is a macroscopic superposition of two eigenstates belonging to different sectors of the spectrum of Hamiltonian (1).

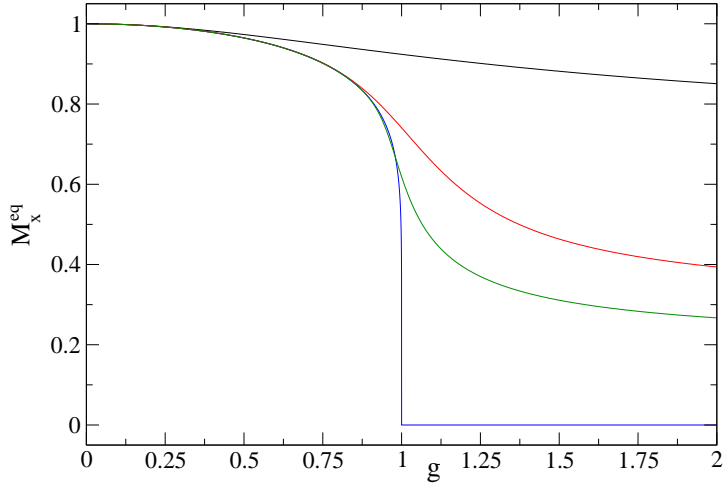


FIG. 1: The equilibrium longitudinal magnetization M_x^{eq} of the quantum Ising chain. The curves, top to bottom, correspond to system sizes 2 (black), 12 (red), 50 (green), and ∞ (blue). The first of them comes from (25), the second (third) one has been numerically obtained in the periodic (open) system, the last one is given by (7).

To understand this statement, we note that commutation of Hamiltonian (1) with the parity operator,

$$P = \prod_{i=1}^N \sigma_i^z, \quad [H, P] = 0, \quad (8)$$

leads to splitting of the Hilbert space into two subspaces, where the eigenstates have either +1 or -1 parity [26]. The symmetry-breaking gap δ is the difference between the energies of the lowest-energy eigenstates in the negative and positive parity subspaces in the ferromagnetic phase, where the symmetry-breaking phenomenon takes place. Such a quantity, however, will be of key importance in our studies for any value of the magnetic field g . We will thus call it the symmetry-breaking gap even when it will be computed at the critical point or in the paramagnetic phase, which will simplify our discussion.

These features of the spectrum are illustrated in Fig. 2. A closed-form expression for δ was given in [26]

$$\delta = g^N \int_0^1 dt \frac{4N}{\pi} \frac{t^{N-3/2} \sqrt{(1-t)(1-g^2t)}}{1-(gt)^{2N}} \quad \text{for } 0 \leq g < 1, \quad (9)$$

$$\delta = 2g - 2 + g^{-N} \int_0^1 dt \frac{4N}{\pi} \frac{t^{N-3/2} \sqrt{(1-t)(g^2-t)}}{1-t^{2N}/g^{2N}} \quad \text{for } g > 1, \quad (10)$$

$$\delta = 2 \tan\left(\frac{\pi}{4N}\right) \quad \text{at } g = 1. \quad (11)$$

These expressions can be used for showing that δ vanishes exponentially (algebraically) with the system size deeply in the ferromagnetic phase (near the critical point) [26]. Deeply in the paramagnetic phase, δ is well-approximated by an expression that is obtained from (10) after neglecting the term containing the integral.

Besides the symmetry-breaking gap, there are also dynamical gaps Δ_+ and Δ_- . They are defined as energy gaps in subspaces of positive and negative parity between the ground state and the first excited state that can be populated during evolution starting from (3)—see Fig. 2. Their

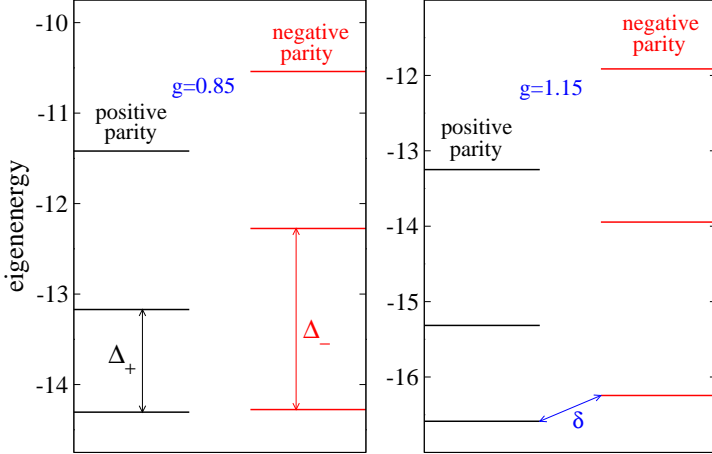


FIG. 2: Lowest-energy levels of Hamiltonian (1) for $N = 12$, which are populated during time evolution starting from state (3) and driven by quench protocol (4). Left panel: typical results in the ferromagnetic phase. The positive and negative parity ground states are nearly degenerate despite the relatively small system size. Right panel: typical results in the paramagnetic phase. The dynamical gaps in the positive and negative parity subspaces, Δ_+ and Δ_- , respectively, and the symmetry-breaking gap δ are marked to illustrate key quantities involved in our studies. Their values for the parameters used in this figure can be found in Table I.

importance comes from the fact that commutation relation (8) prohibits dynamical transitions between the two parity subspaces. As a result, system's excitation due to driving (4) depends on Δ_{\pm} , the quench time τ_Q , and the initial state (3) for time evolution. It has nothing to do with the symmetry-breaking gap δ as long as there is no symmetry-breaking perturbation in the system, which is the case in our studies.

If we now note that $\sigma^z |\rightarrow\rangle = |\leftarrow\rangle$, which implies $\sigma^z |\leftarrow\rangle = |\rightarrow\rangle$, we see that the ground states in the positive- and negative-parity subspaces at $g = 0$ can be written as

$$|GS_{\pm}(g=0)\rangle = \frac{|\rightarrow\rightarrow\rightarrow\cdots\rangle \pm |\leftarrow\leftarrow\leftarrow\cdots\rangle}{\sqrt{2}}, \quad (12)$$

which in turn allows us to cast initial state (3) to the following form

$$|\psi(t=0)\rangle = \frac{|GS_+(g=0)\rangle + |GS_-(g=0)\rangle}{\sqrt{2}}. \quad (13)$$

Next, we use (8) and employ time-dependent Schrödinger equation to arrive at

$$\begin{aligned} |\psi(t)\rangle &= |\psi_+(t)\rangle + |\psi_-(t)\rangle, \\ P|\psi_{\pm}(t)\rangle &= \pm|\psi_{\pm}(t)\rangle. \end{aligned} \quad (14)$$

Finally, knowing that σ_i^x has vanishing matrix elements in positive- and negative-parity subspaces, we get

$$M_x(t) = \langle\psi(t)|\sigma_i^x|\psi(t)\rangle = \langle\psi_-(t)|\sigma_i^x|\psi_+(t)\rangle + \text{c.c.} \quad (15)$$

This expression can be very complicated for fast quenches, i.e., for small τ_Q in (4). However, if we assume that the driving is slow enough to be nearly adiabatic, then the following expression will properly approximate the exact result

$$M_x(t) = \cos\left(\int_{-g_f\tau_Q}^t dt \delta[g(t)]\right) \langle GS_-[g(t)]|\sigma_i^x|GS_+[g(t)]\rangle. \quad (16)$$

Such an expression is still non-trivial because we are unaware of a closed-form expression for the above matrix element in an arbitrarily-sized system. If we now consider $t > 0$, i.e., the free evolution stage in our problem, we will get from (16) that

$$M_x(t) = \cos(\delta(g_f)t + \text{const}) M_x^{eq}(g_f), \quad (17)$$

which can be used for extracting the symmetry-breaking gap and the equilibrium longitudinal magnetization out of either numerical or experimental data.

The question now is what is the condition for adiabaticity in our system so that approximation (16) can be used. Clearly, the system is most prone to being excited near the critical point, where the dynamical gap Δ_{\pm} is smallest, and the quantum version [8, 9, 27] of the Kibble-Zurek (KZ) theory of non-equilibrium phase transitions [28–31] can be used. A simple criteria then exists and is based on comparision between the system size and the non-equilibrium length-scale $\hat{\xi}$ characterizing excitations resulting from the quench [32]. The latter, according to the KZ theory, scales with the quench time as

$$\hat{\xi} \sim \tau_Q^{\nu/(1+z\nu)}, \quad (18)$$

where z and ν are the critical exponents. These exponents describe disappearance of the dynamical gap and the correlation length, which are assumed to be proportional to $|g - g_c|^{z\nu}$ and $|g - g_c|^{-\nu}$, respectively, near the critical point g_c . Comparing the two length scales, one gets the following condition for a crossover between adiabatic and non-adiabatic evolutions approaching or crossing the critical point

$$\tau_Q \sim N^{(1+z\nu)/\nu} \sim N^2, \quad (19)$$

where we substituted $z = \nu = 1$ for the quantum Ising model in the transverse field. In other words, for quench times of the order of N^2 or larger we expect the evolution to be nearly adiabatic.

The outline of this paper is the following. We illustrate in Sec. II the above concepts related to the symmetry-breaking gap and the equilibrium longitudinal magnetization in the simplest version of the Ising model composed of just two spins. We then discuss in Sec. III dynamical extraction of those quantities from after-quench free evolution of the longitudinal magnetization in the periodic Ising chain composed of several spins. Next, we extend these studies in Sec. IV to systems composed of up to several hundreds of spins by considering open Ising chains, where computations of the longitudinal magnetization can be more efficiently done. Finally, the overall discussion of our results is presented in Sec. V.

II. TWO SPINS

We illustrate in this section how longitudinal magnetization can be calculated in the simplest version of the Ising chain, the one with just two spins.

To start, we need eigenenergies and normalized eigenstates of (1), which for $N = 2$ read

$$\mathcal{E}_{GS_+} = -2\sqrt{1+g^2}, \quad |GS_+\rangle = A_-|\uparrow\uparrow\rangle + B_-|\downarrow\downarrow\rangle, \quad (20)$$

$$\mathcal{E}_{GS_-} = -2, \quad |GS_-\rangle = \frac{|\uparrow\downarrow\rangle + |\downarrow\uparrow\rangle}{\sqrt{2}}, \quad (21)$$

$$\mathcal{E}_{EX_-} = 2, \quad |EX_-\rangle = \frac{|\uparrow\downarrow\rangle - |\downarrow\uparrow\rangle}{\sqrt{2}}, \quad (22)$$

$$\mathcal{E}_{EX_+} = 2\sqrt{1+g^2}, \quad |EX_+\rangle = A_+|\uparrow\uparrow\rangle + B_+|\downarrow\downarrow\rangle, \quad (23)$$

	δ	Δ_+	Δ_-	M_x^{eq}
$g = 0.85$	0.028747	1.13	2.00	0.8545
$g = 1$	0.13109	1.04	2.07	0.7407
$g = 1.15$	0.34167	1.27	2.30	0.6146

TABLE I: The symmetry-breaking gap δ , the dynamical gaps Δ_{\pm} , and the equilibrium magnetization M_x^{eq} in the periodic Ising chain composed of $N = 12$ spins.

where $\sigma^z|\uparrow\rangle = |\uparrow\rangle$, $\sigma^z|\downarrow\rangle = -|\downarrow\rangle$,

$$A_{\pm} = \frac{1}{\sqrt{2}\sqrt{1+g^2 \pm g\sqrt{1+g^2}}}, \quad B_{\pm} = -\frac{g \pm \sqrt{1+g^2}}{\sqrt{2}\sqrt{1+g^2 \pm g\sqrt{1+g^2}}}, \quad (24)$$

and EX_{\pm} refers to excited states in the corresponding subspaces.

It is then a standard exercise to show that the extremal values of longitudinal magnetization in the state, which is an arbitrary superposition of $|GS_+\rangle$ and $|GS_-\rangle$, are

$$\begin{aligned} M_x &= \pm \langle GS_- | \sigma_i^x | GS_+ \rangle = \pm M_x^{eq} \\ &= \pm \frac{1}{2} \left(\sqrt{1 + \frac{g}{\sqrt{1+g^2}}} + \sqrt{1 - \frac{g}{\sqrt{1+g^2}}} \right). \end{aligned} \quad (25)$$

This formula is depicted in Fig. 1, where one easily notices its departures from thermodynamic limit expression (7). These differences do not vanish in the whole paramagnetic phase. In fact, for a periodic system composed of N spins, it is easy to show that the longitudinal magnetization does not vanish even in the limit of $g \rightarrow \infty$

$$M_x^{eq}(g \rightarrow \infty) = \frac{1}{\sqrt{N}}. \quad (26)$$

Such a simple result follows from elementary observation that for $g \rightarrow \infty$ the positive-parity ground state is $|\uparrow\uparrow\uparrow\uparrow\cdots\rangle$, while the negative-parity one reads

$$\frac{|\downarrow\uparrow\uparrow\uparrow\cdots\rangle + |\uparrow\downarrow\uparrow\uparrow\cdots\rangle + |\uparrow\uparrow\downarrow\uparrow\cdots\rangle + \cdots}{\sqrt{N}}. \quad (27)$$

III. DYNAMICS OF THE PERIODIC CHAIN

We will discuss here dynamics of the longitudinal magnetization in a periodic Ising chain with $N \gg 2$. There are different ways how one can approach this problem.

The most direct way is to work in the Fock space spanned by all combinations of up/down states of all spins such as $|\uparrow\downarrow\downarrow\uparrow\cdots\rangle$. Such a Fock space can be then easily cut into positive and negative parity subspaces, where either time evolutions or diagonalizations used for getting equilibrium value of the longitudinal magnetization can be independently performed. The advantage of such an approach is that it allows for easy computation of the longitudinal magnetization. The disadvantage is rather obvious: one has to keep track of $2 \times 2^{N-1}$ amplitudes, which highly limits the available system sizes.

Another approach relies on mapping the system onto non-interacting fermions via the Jordan-Wigner transformation

$$\begin{aligned} \sigma_i^z &= 1 - 2c_i^\dagger c_i, \quad \sigma_i^x = (c_i + c_i^\dagger) \prod_{j < i} (1 - 2c_j^\dagger c_j), \\ \{c_i, c_j^\dagger\} &= \delta_{ij}, \quad \{c_i, c_j\} = 0, \end{aligned} \quad (28)$$

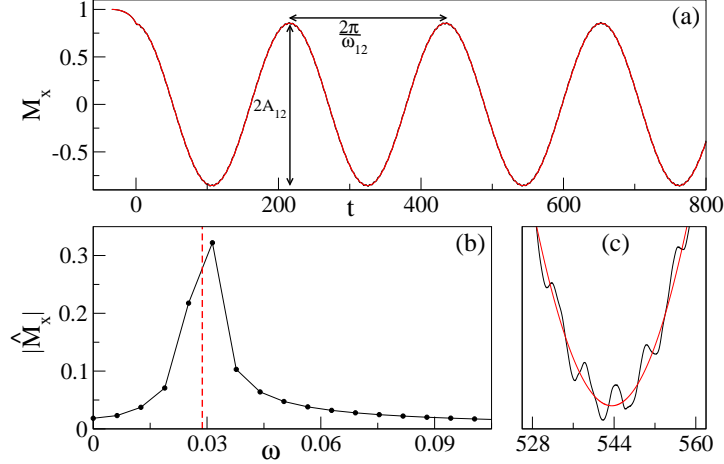


FIG. 3: Dynamics of the longitudinal magnetization in a periodic system for a nearly adiabatic quench that stops in the ferromagnetic phase at $g_f = 0.85$. Panel (a): the black line shows numerics, while the red one shows adiabatic approximation (16). Panel (b): modulus of the discrete Fourier transform (40) of free evolution of the longitudinal magnetization around the symmetry-breaking gap δ marked by the vertical red dashed line. Data points are joined by line segments to guide the eye. Panel (c): magnification of the area around the third minimum from panel (a). The system size is $N = 12$, the quench time is $\tau_Q = 40$, and the time span of free oscillations used for computing (40) is $L = 1000$ (the S parameter from (40) is of the order of a few tens of thousands in all our studies, its exact value is of marginal use in the following discussion).

after which the Hamiltonian can be diagonalized if we transform fermionic operators to the Fourier basis

$$c_j = \frac{e^{-i\pi/4}}{\sqrt{N}} \sum_k c_k e^{ikj}, \quad (29)$$

properly quantize momenta k , and make use of the Bogolubov transformation. The key observation, in the context of our discussion, is that different momenta have to be chosen in the positive and negative parity subspaces,

$$k_+ = \pm \frac{\pi}{N}, \pm \frac{3\pi}{N}, \dots, \pm \frac{N-1}{N}\pi, \quad (30)$$

and

$$k_- = 0, \pm \frac{2\pi}{N}, \pm \frac{4\pi}{N}, \dots, \pm \frac{N-2}{N}\pi, \pi, \quad (31)$$

respectively. These expressions are valid for even N , which we assume in this section (see [26] for comprehensive discussion of the Ising diagonalization intricacies).

Combining the results of [8] and [26], time-dependent wave-function (14) can be obtained from

$$|\psi_+(t)\rangle = \prod_{k_+ > 0} \left(u_{k_+}(t) - v_{k_+}(t) c_{k_+}^\dagger c_{-k_+}^\dagger \right) |\text{vac}\rangle, \quad (32)$$

$$|\psi_-(t)\rangle = e^{-2it} c_0^\dagger \prod_{0 < k_- < \pi} \left(u_{k_-}(t) - v_{k_-}(t) c_{k_-}^\dagger c_{-k_-}^\dagger \right) |\text{vac}\rangle, \quad (33)$$

where e^{-2it} accounts for evolution of the zero-momentum mode, which is occupied and uncoupled from other modes [26]. The state $|\text{vac}\rangle$ is annihilated by all c_k operators and time-evolution of the

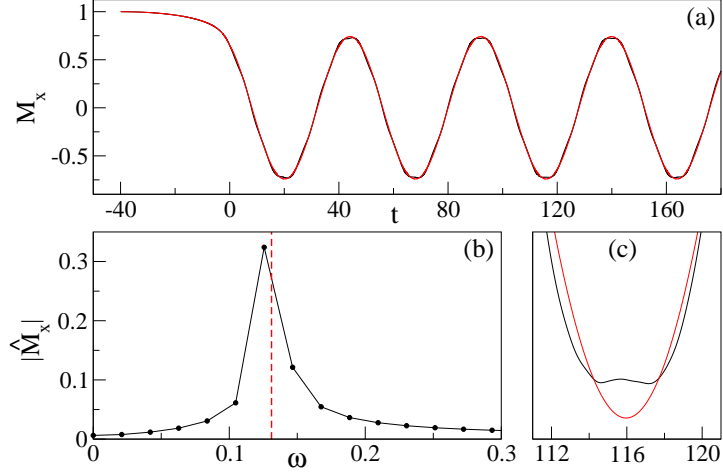


FIG. 4: Dynamics of the longitudinal magnetization in a periodic system for a nearly adiabatic quench that stops at the critical point. This figure is organized in the same way as Fig. 3. The parameters are $g_f = 1$, $N = 12$, $\tau_Q = 40$, and $L = 300$.

Bogolubov modes is governed by

$$i \frac{d}{dt} \begin{pmatrix} v_k \\ u_k \end{pmatrix} = 2 \begin{pmatrix} g - \cos(k) & -\sin(k) \\ -\sin(k) & \cos(k) - g \end{pmatrix} \begin{pmatrix} v_k \\ u_k \end{pmatrix}. \quad (34)$$

Having (34) at hand, one can find by diagonalization of the 2×2 Hamiltonian that the energy gap for excitation of the pair of $\pm k$ fermionic modes is

$$4\sqrt{g^2 - 2g \cos(k) + 1}. \quad (35)$$

The smallest value of that gap in each of the parity subspaces is the dynamical gap Δ_{\pm} , which we have already introduced in Sec. I—see also Fig. 2. Thereby,

$$\Delta_+ = 4\sqrt{g^2 - 2g \cos(\pi/N) + 1}, \quad \Delta_- = 4\sqrt{g^2 - 2g \cos(2\pi/N) + 1}. \quad (36)$$

From the above expressions, it is clear that time evolution of our system can be obtained after solving $N - 2$ uncoupled two-level systems. This is the most efficient way of getting wave-function (14). The problem with this approach, however, lies in the complexity of the computation of M_x , which in our periodic system can be written as

$$M_x = \langle \psi_-(t) | c_1 + c_1^\dagger | \psi_+(t) \rangle + \text{c.c.} \quad (37)$$

Indeed, if we put (32) and (33) into (37) and then transform $c_{k\pm}$ operators to the position space inverting (29)—so that all operators are defined on the same Hilbert space—we will quickly realize how complicated the resulting expression is.

We will thus use the first above-mentioned approach, i.e., the direct numerical solution, to characterize dynamics of the $N = 12$ periodic chain. In the next section, we will sacrifice the translational invariance by doing calculations in much larger open chains, where such problems with computation of the longitudinal magnetization are absent.

The results of our numerical simulations are presented in Figs. 3–5, where we have chosen quench time τ_Q large-enough to ensure that evolutions will be nearly adiabatic. We see there that after stopping the quench, say for

$$0 \leq t \leq L, \quad (38)$$

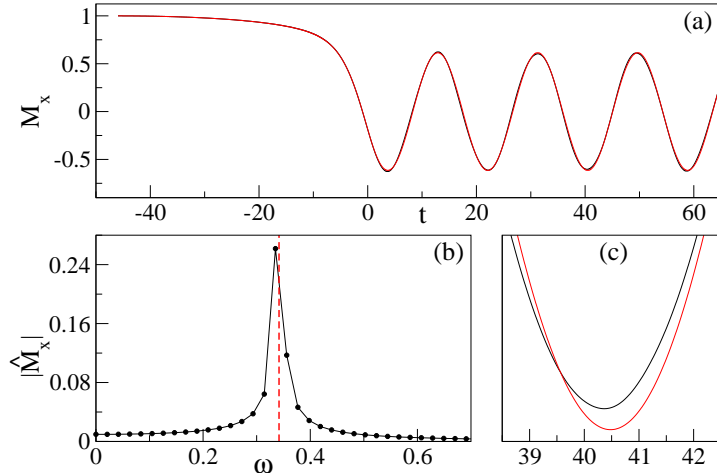


FIG. 5: Dynamics of the longitudinal magnetization in a periodic system for a nearly adiabatic quench that stops in the paramagnetic phase. This figure is organized in the same way as Fig. 3. The parameters are $g_f = 1.15$, $N = 12$, $\tau_Q = 40$, and $L = 300$.

there are periodic oscillations, which will be studied in various ways.

First, we will extract from numerical data the difference between positions of the first two maxima of $M_x(t)$ and use it to compute the frequency ω_{12} of oscillations. We will also get from such data half of the difference between $M_x(t)$ in the first maximum and the second minimum to obtain the oscillation amplitude A_{12} . These quantities are illustrated in Fig. 3. The frequency ω_{12} and amplitude A_{12} estimate $\delta(g_f)$ and $M_x^{eq}(g_f)$ —see (17) for justification of this statement¹. As far as numerical simulations are concerned, the uncertainty of getting ω_{12} and A_{12} is negligible. This is perhaps the easiest way of characterization of after-quench oscillations as it requires observation of no more than two oscillation periods.

Second, we will fit the periodic function

$$M_x(t) = A_{\text{fit}} \cos(\omega_{\text{fit}} t + \text{const}) \quad (39)$$

expecting that ω_{fit} and A_{fit} will estimate the same physical quantities as ω_{12} and A_{12} . Such fitting will be done with NonlinearModelFit function from [33]. This function also provides uncertainty of the fitted parameters, which is negligible in our studies of ω_{fit} and A_{fit} . A few oscillation periods provide enough data for reaching the full potential of this technique.

Third, we will compute the discrete Fourier transform

$$\hat{M}_x(\omega_j) = \frac{1}{S} \sum_{s=0}^{S-1} M_x(s\Delta t) e^{i\omega_j s\Delta t}, \quad (40)$$

$$\Delta t = \frac{L}{S}, \quad \omega_j = \frac{2\pi j}{L}, \quad j = 0, 1, \dots, S-1$$

looking for the position ω_{max} of the global maximum of $|\hat{M}_x|$ also estimating the symmetry-breaking gap. The advantage of this technique, over the above-mentioned ones, is that it allows for detection of the whole spectrum of frequencies without assuming that there is just one frequency. The problematic thing, however, is that one needs long “observation” times L to reach high accuracy

¹ Note that we work with $\hbar = 1$, where the frequency and the energy can be directly compared.

	ω_{12}	ω_{\max}	ω_{fit}	A_{12}	A_{fit}
$g_f = 0.85$	0.028422	0.031416	0.028747	0.8620	0.8538
$g_f = 1$	0.13114	0.12566	0.13108	0.7286	0.7397
$g_f = 1.15$	0.34177	0.33510	0.34174	0.6178	0.6146

TABLE II: Parameters describing free oscillations of the longitudinal magnetization from Figs. 3 to 5 (top to bottom). Symbols ω_{12} , ω_{\max}, \dots , A_{fit} are defined around equations (39) and (40). The fitting leading to ω_{fit} and A_{fit} has been done on time intervals $0 \leq t \leq 4 \times 2\pi/\delta(g_f)$ corresponding to four oscillation periods during free evolution.

because the spectral resolution of the discrete Fourier transform is

$$2\pi/L. \quad (41)$$

This is seen in Figs. 3b–5b, where the horizontal spacing between the data points ranges between 0.006 and 0.02, which is non-negligible relative to the symmetry-breaking gap that we try to extract from such data.

We have applied all these techniques to numerics from Figs. 3a–5a getting results that are presented in Table II. We see there very good agreement between the oscillation frequencies ω_{12} , ω_{\max} , ω_{fit} and the value of the symmetry-breaking gap δ from Table I. Moreover, similar agreement is found between the oscillation amplitudes A_{12} , A_{fit} and M_x^{eq} also listed in that table.

Such a good agreement is a result of choosing so large quench time τ_Q , that evolutions are nearly adiabatic (Figs. 3a–5a). If we now take a look at Figs. 3c–5c, we will be able to notice small deviations from the perfectly adiabatic solution (16). Similar features will be seen in the simulations of the open chains, which brings us to the next section of this work, where they will be discussed.

IV. DYNAMICS OF THE OPEN CHAIN

We will study in this section dynamics of the open Ising chain described by the following Hamiltonian

$$\tilde{H}(g) = - \sum_{i=1}^{N-1} \sigma_i^x \sigma_{i+1}^x - \sum_{i=1}^N g \sigma_i^z. \quad (42)$$

While such a Hamiltonian seems to be nearly identical to the one used in the previous sections, time evolution of the wave-function in the open chain is significantly more complicated than in the periodic one. Therefore, consideration of the open chain may, at first glance, look like a step backwards with respect to the studies from Sec. III. This is not the case for at least two reasons.

First, open chains are more experimentally-relevant than the periodic ones as it is a very complicated task to engineer a periodic coupling between the spins (see e.g. [34] for an elaborate proposal how this might be achieved in a cold ion simulator of spin systems).

Second, computations of the longitudinal magnetization can be much more efficiently done in the open chain. It is so because the parity operator (8) does not appear during the diagonalization of Hamiltonian (42) and so there is no need to work in definite-parity subspaces of the Hilbert space, which was complicating calculations in Sec. III. This allows for efficient evaluation of the longitudinal magnetization in systems composed of up to a few hundreds of spins, which is a major step forward with respect to our studies of periodic chains. This flexibility with respect to the system size allows us for systematic studies of the transition from the non-equilibrium regime,

	E_1	E_2	E_3	E_4	E_5	E_6	E_7
$g_f = 1, N = 50$	0.0622	0.187	0.311	0.435	0.558	0.681	0.803
$g_f = 0.85, N = 20$	0.0217	0.470	0.730				
$g_f = 1.15, N = 50$	0.322	0.383	0.470				

TABLE III: Energies of single-particle excitations relevant for deciphering the positions of marked maxima in Figs. 6, 7, and 9.

	M_x^{eq}
$g = 0.85, N = 20$	0.8448
$g = 1, N = 50$	0.6188
$g = 1.15, N = 50$	0.4204

TABLE IV: The equilibrium longitudinal magnetization in the open Ising chain for the parameters relevant to the studies reported in Figs. 6–8.

where the Kibble-Zurek theory describes the system’s excitation, to the nearly adiabatic regime, which we have already begun to investigate in Sec. III.

Moving on to the actual calculations, we mention that technical details related to diagonalization of Hamiltonian (42) and time evolution that it generates are presented in Appendix A. We only summarize here some basic formulae that are necessary for understanding of the following discussion.

After Jordan-Wigner mapping (28), the Hamiltonian is diagonalized by the Bogolubov transformation so that it finally reads

$$\begin{aligned} \tilde{H} &= \sum_{i=1}^N E_i \left(\gamma_i^\dagger \gamma_i - 1/2 \right), \\ \{\gamma_i, \gamma_j^\dagger\} &= \delta_{ij}, \quad \{\gamma_i, \gamma_j\} = 0, \end{aligned} \quad (43)$$

where the energies of single-particle excitations are sorted in ascending order: $E_1 \leq E_2 \leq \dots \leq E_N$. This means that the symmetry-breaking gap is given by

$$\delta = E_1. \quad (44)$$

We obtain E_i ’s numerically. The results, relevant for the subsequent discussion, are collected in Table III.

Besides the symmetry-breaking gap, we are also interested in the longitudinal magnetization, which is now position dependent. Its equilibrium value in the open Ising chain was recently discussed in [35], where it was analyzed how the “ends” of the chain affect its value. To minimize their influence on our results, we will focus our attention on the center of the system by calculating

$$M_x = \langle \sigma_{N/2}^x \rangle. \quad (45)$$

The equilibrium values of such defined longitudinal magnetization, for the parameters relevant for the subsequent discussion, are listed in Table IV. The technical details of computation of (45) are discussed in Appendix A. An important thing now is to note that if we write the Schrödinger-picture wave-function at the time the quench stops as

$$\begin{aligned} |\psi(t=0)\rangle &= \sum_{i_1 i_2 \dots i_N} a_{i_1 i_2 \dots i_N} |i_1 i_2 \dots i_N\rangle, \\ |i_1 i_2 \dots i_N\rangle &= \left(\gamma_1^\dagger \right)^{i_1} \left(\gamma_2^\dagger \right)^{i_2} \dots \left(\gamma_N^\dagger \right)^{i_N} |GS\rangle, \\ i_n &= 0, 1 \text{ and } \gamma_n |GS\rangle = 0 \text{ for } 1 \leq n \leq N, \end{aligned} \quad (46)$$

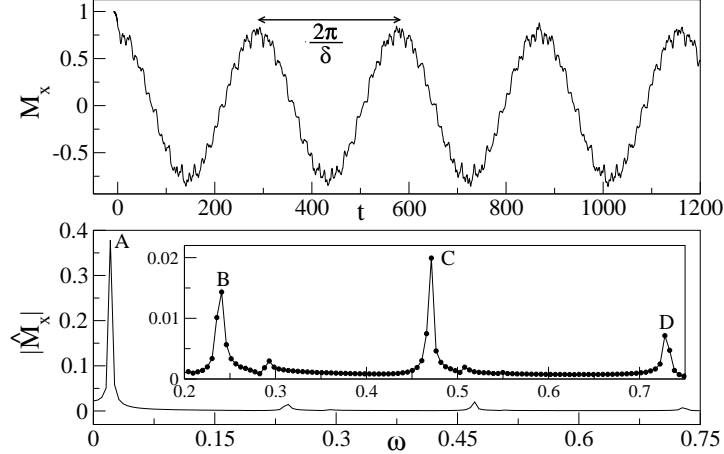


FIG. 6: Upper panel: dynamics of the longitudinal magnetization in the open Ising chain for the quench that stops in the ferromagnetic phase. The parameters are $g_f = 0.85$, $N = 20$, and $\tau_Q = 10$. δ is given by E_1 from Table III (second row). Lower panel: modulus of the discrete Fourier transform of free evolution data, i.e. $M_x(t > 0)$, from the upper panel. The inset enlarges peaks B–D. $L = 1200$ has been used to compute the transform.

where the amplitudes $a_{i_1 i_2 \dots i_N}$'s are such that the wave-function is normalized to unity, then at times $t > 0$

$$M_x(t) = \sum_{\substack{j_1 j_2 \dots j_N \\ i_1 i_2 \dots i_N}} \overline{a_{j_1 j_2 \dots j_N}} a_{i_1 i_2 \dots i_N} e^{it \sum_{n=1}^N (j_n - i_n) E_n} \langle j_1 j_2 \dots j_N | \sigma_{N/2}^x | i_1 i_2 \dots i_N \rangle \quad (47)$$

with

$$\sum_{n=1}^N (i_n + j_n) \text{ being odd.} \quad (48)$$

If this condition is not satisfied, then the matrix element in (47) identically vanishes, which can be shown with Wick's theorem. This feature impacts Fourier spectra of the longitudinal magnetization.

A. Quenches stopping in ferromagnetic or paramagnetic phase

We start discussion of our numerical simulations from the non-equilibrium quench that has been stopped in the ferromagnetic phase (Fig. 6). The first thing that catches our attention in this figure is “roughness” of free evolution of M_x . To understand it, we need to look at modulus of its discrete Fourier transform.

By doing so, we first notice a series of peaks enumerated by A , B , etc. whose maxima are placed at ω_A , ω_B , etc. listed in Table V. If we now use data from Table III and equations (47) and (48), we can note that within spectral resolution of the Fourier transform ω_A , ω_B , ω_C , and ω_D can be identified with E_1 , $E_3 - E_1 - E_2$, E_2 , and E_3 , respectively. Quite interestingly, the B peak can be linked to the two-particle excitation. The other peaks come from single-particle excitations, which is, of course, an expected feature.

Occupation of the Fourier modes around ω_A is responsible for the oscillation period $2\pi/\delta(g_f)$ marked in the upper panel of Fig. 6. Next, we note that (i) ω_B , ω_C , etc. are larger by at least a factor of ten than ω_A and (ii) $|\hat{M}_x(\omega_A)|$ is larger by at least a factor of fifteen than $|\hat{M}_x(\omega_B)|$, $|\hat{M}_x(\omega_C)|$,

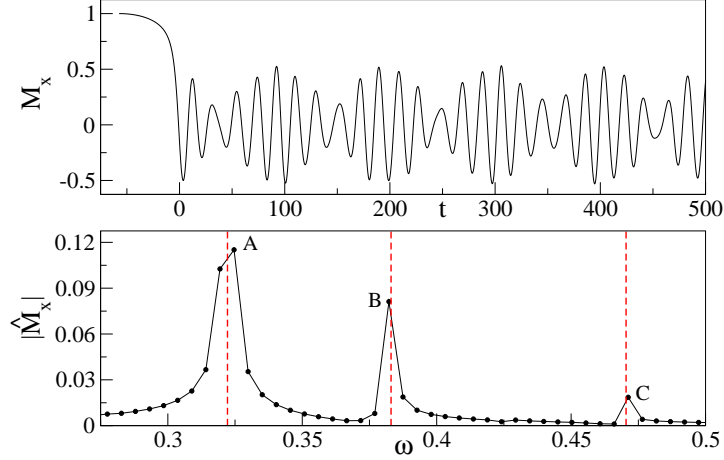


FIG. 7: Upper panel: dynamics of the longitudinal magnetization in the open Ising chain for the quench that stops in the paramagnetic phase. The parameters are $g_f = 1.15$, $N = 50$, and $\tau_Q = 50$. Lower panel: modulus of the discrete Fourier transform of the free evolution data from the the upper panel. The vertical red dashed lines in the lower panel show energies of the single-particle excitations from the third row of Table III. $L = 1200$ has been used to compute the transform.

etc. The (i) observation means that there will be high frequency oscillations on top of the base oscillation, whose frequency is approximated by ω_A . The (ii) remark implies that they will have small amplitude relative to the amplitude of the base oscillation. Both features are nicely seen in the upper panel of Fig. 6.

A quite different situation is encountered when the quench stops in the paramagnetic phase. This is illustrated in Fig. 7, where we see beats. A simple explanation of this observation comes again from the discrete Fourier transform, where we see two leading peaks centered around ω_A and ω_B . The beats result from the fact that $|\hat{M}_x(\omega_A)|$ is comparable to $|\hat{M}_x(\omega_B)|$. Moreover, we note that ω_A , ω_B , and ω_C are of the same order of magnitude, which eliminates high frequency oscillations seen in Fig. 6. Looking more quantitatively at the Fourier transform from Fig. 7, we notice that ω_A , ω_B , and ω_C can be identified with E_1 , E_2 , and E_3 within the spectral resolution of the Fourier transform (Tables III and V).

Finally, at the risk of stating the obvious, we mention that we recover adiabatic results, akin to those presented in Figs. 3 and 5, by increasing the quench times from Figs. 6 and 7. In the opposite limit of fast transitions, free evolution of the longitudinal magnetization becomes noisy and so less interesting in the context of our studies.

B. Quenches to critical point

We will discuss now the transition to the adiabatic regime for evolutions ending at the critical point. Such evolutions are depicted in Fig. 8. For small τ_Q , we see a train of narrow peaks, whose amplitude decreases as time goes by. The magnetization in between the peaks is nearly zero. As evolutions slow down, the decay of the peaks' amplitude slows and the peaks' width increases shrinking time intervals, where the system is unmagnetized in the longitudinal direction. By the time those intervals disappear, the curve describing dynamics of the longitudinal magnetization has a triangular-like shape. Further increase of the quench time brings the expected single-frequency dynamics characteristic of the adiabatic evolution (17).

The rather unusual shape of oscillations of the longitudinal magnetization for the fastest quenches from Fig. 8 comes from substantial population of several Fourier modes. This is illustrated in Fig.

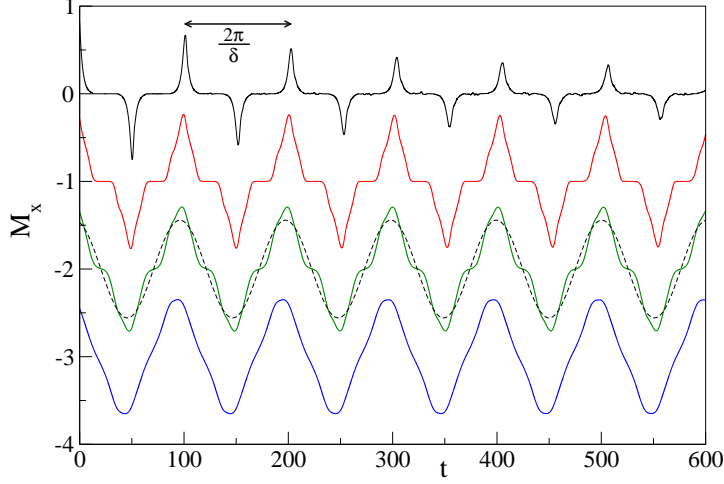


FIG. 8: Free evolution of the longitudinal magnetization after quenches to the critical point in the open Ising chain. The solid curves, from top to bottom, correspond to $\tau_Q = 2$ (black), $\tau_Q = 20$ (red), $\tau_Q = 73$ (green), and $\tau_Q = 200$ (blue). The subsequent curves are shifted downward by a multiple of 1 to facilitate their comparison. The dashed black curve shows $0.557 \cos(0.0622t + 0.307)$ shifted downward by 2. It comes from the fit to the numerics for $\tau_Q = 73$, which is close to the crossover quench time discussed in Fig. 10. The parameters are $g_f = 1$ and $N = 50$. δ is given by E_1 from Table III (first row).

9, where the subsequent Fourier peaks are centered at the energies of consecutive single-particle excitations (Tables III and V).

Moreover, we see in Fig. 8 that the period of oscillations is approximately given by $2\pi/\delta$. It can be shown to be well-approximated by $2N$ at the critical point (A4), where free evolution takes place. This timescale is even easily seen in the dynamics of the fastest quench from Fig. 8, which is quasi-periodic. It is twice smaller than the oscillation period at the critical point of the periodic system, which can be trivially shown with (11). The linear dependence of the oscillation period on the system size, albeit with a different prefactor, was also observed in our earlier studies of the quantum Ising model [23], where we investigated free dynamics of the transverse magnetization after quenches moving the system from the paramagnetic phase to the critical point. Except for the similarly in the repetition period, quite different dynamics is observed there.

To study quantitatively the crossover from the non-equilibrium to the adiabatic regime, which we depict in Fig. 8, we need some measure of the deviation of non-equilibrium evolution from the adiabatic limit. A good measure should be easily numerically and experimentally accessible. It should be also stable against fluctuations of the data for $M_x(t)$. Several options seem to be available.

First, one may analyze modulus of the discrete Fourier transform. For example, one can study how the global maximum around the symmetry-breaking gap grows with increasing τ_Q . Alternatively, one may research how the other extrema disappear in such a limit. This choice, however, is problematic. As the main obstacle, we see limitations imposed by the spectral resolution of the discrete Fourier transform (41). To overcome them, either long free evolution times are needed or some fitting procedure allowing for precise interpolation of the properties of extrema of $|\hat{M}_x|$ from sparse data. This is a complication affecting both numerical and experimental studies. The latter would be also affected by the fact that the Fourier transform is not directly measured and so its extraction out of $M_x(t)$ will necessarily bring some inaccuracies that may play a role in the Kibble-Zurek scaling analysis.

Second, one may use a more straightforward approach by studying the amplitude and spacing

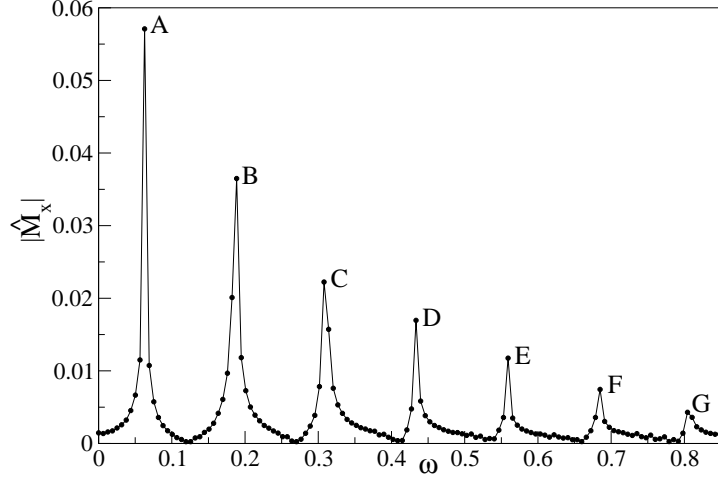


FIG. 9: Modulus of the discrete Fourier transform of free evolution of the longitudinal magnetization of the fastest quench from Fig. 8: $g_f = 1$, $N = 50$, $\tau_Q = 2$. $L = 1000$ is used to compute the transform.

	ω_A	ω_B	ω_C	ω_D	ω_E	ω_F	ω_G
$g_f = 1$, $N = 50$	0.0628	0.188	0.308	0.434	0.559	0.685	0.804
$g_f = 0.85$, $N = 20$	0.0209	0.241	0.471	0.728			
$g_f = 1.15$, $N = 50$	0.325	0.382	0.471				

TABLE V: The positions of maxima of $|\hat{M}_x|$ marked in Figs. 6, 7, and 9.

of the first two peaks of $M_x(t)$, just as in Sec. III. Such a method, however, is susceptible to fluctuations of the data. This can be improved by averaging results collected for several peaks, but this would again require long free evolution times, which is problematic.

Third, one may fit (39) to free evolution of the longitudinal magnetization and study such obtained amplitude of oscillations A_{fit} (Fig. 10). Such a procedure uses all information contained in $M_x(t)$ —not only the one stored in the extrema of either M_x or $|\hat{M}_x|$ —and so long evolution times are not needed. Moreover, it should work well with irregular data averaging out the fluctuations, which is of interest in the context of high-precision numerical and experimental research. This is the approach that we will employ.

Before moving on, we again mention that the fitted amplitude A_{fit} converges to $M_x^{\text{eq}}(g_f)$ in the adiabatic limit. For faster quenches, however, it underestimates the real amplitude of oscillations, which is seen in Fig. 8. This has no effect on our studies, which is perhaps best illustrated by the excellent agreement between the scaling exponent extracted out of the fitted amplitude and the predictions of the Kibble-Zurek theory (see below).

To proceed, we define the crossover quench time τ_Q^{cross} by the condition

$$\left| \frac{A_{\text{fit}}(\tau_Q) - M_x^{\text{eq}}(g_f)}{M_x^{\text{eq}}(g_f)} \right| < \eta \quad \text{for } \tau_Q > \tau_Q^{\text{cross}}, \quad (49)$$

where η is the threshold set on the relative difference between the fitted amplitude of oscillations and its asymptotic in τ_Q value. We will use in this formula the amplitude obtained by fitting (39) to $M_x(t)$ for $0 \leq t \leq 12N$, which corresponds to roughly 6 oscillation periods in the open chain. Moreover, we will set $\eta = 10\%$, which should be large-enough to be experimentally-relevant and small-enough to describe the crossover to the adiabatic limit.

Our results for A_{fit} , in the experimentally-relevant system composed of $N = 50$ spins [36, 37],

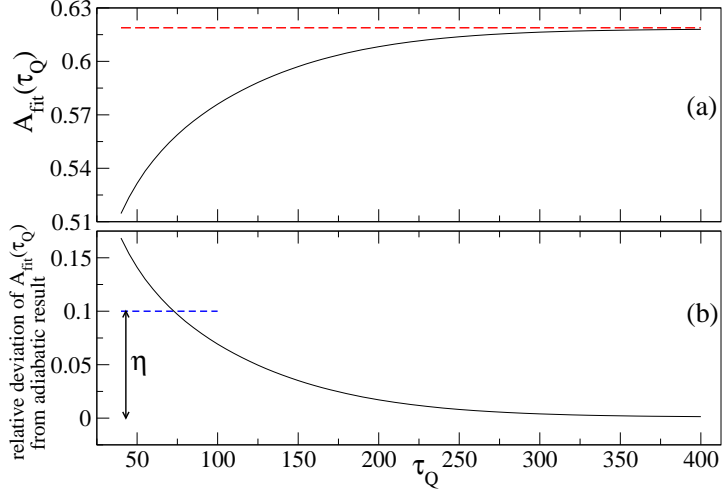


FIG. 10: Panel (a): the fitted amplitude of oscillations of the longitudinal magnetization after stopping the quench at the critical point of the open Ising chain. The solid black line shows numerics in both panels. The dashed red line shows the result for perfectly adiabatic evolution to the critical point, which is given by the equilibrium magnetization (second row of Table IV). Panel (b): the left-hand side of (49). The dashed blue line shows the threshold $\eta = 10\%$ from (49). Its intersection with the solid black line gives $\tau_Q^{\text{cross}} \approx 72.83$. The system size is $N = 50$.

are presented in Fig. 10a, where we see that the fitting procedure produces a perfectly smooth curve monotonically approaching $M_x^{eq}(g_f)$. The threshold η is illustrated in Fig. 10b.

Repeating such analysis for system sizes $20 \leq N \leq 300$, we have obtained detailed results for the crossover quench time τ_Q^{cross} , which we present in Fig. 11a. As we anticipate from (19) that

$$\tau_Q^{\text{cross}}(N) \sim N^a, \quad (50)$$

where $a > 0$ is the scaling exponent, we display results for τ_Q^{cross} on a double logarithmic plot in Fig. 11b. Instead of a straight line, we find in this figure a curve slightly bending upwards as the system size grows. This means that the exponent a increases with N . To quantify this observation, we fit

$$\ln \tau_Q^{\text{cross}} = a \ln N + b \quad (51)$$

to numerical data from four different ranges of the system sizes. The results are collected in Table VI, where we see that a approaches the value of 2 for the largest system sizes that we consider. This is in a very good agreement with the Kibble-Zurek scaling argument (19), which is supposed to work best in the large-system limit. Finally, we notice that the increase of a with N is monotonic, leaving no doubts about stability of the procedure of extraction of τ_Q^{cross} from the free evolution data for the longitudinal magnetization.

V. DISCUSSION

The goal of this work was to investigate how the symmetry-breaking gap, which is of crucial importance in the discussion of quantum phase transitions, can be studied with the help of quantum quenches. We have chosen for this purpose an exactly solvable model, the quantum Ising model in the transverse field, and analyzed its dynamics after quenches induced by the gradual change of the magnetic field. These quenches start from the easy-to-prepare broken-symmetry ground state

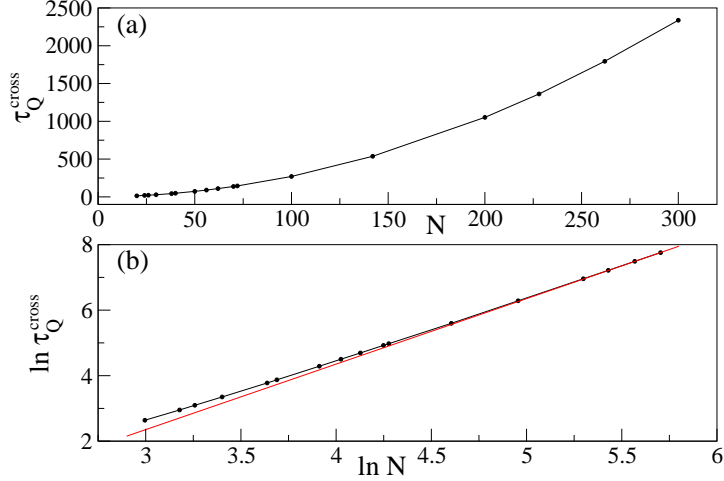


FIG. 11: Panel (a): the crossover quench time τ_Q^{cross} as a function of the system size for quenches that stop at the critical point of the open Ising chain ($g_f = 1$). Dots come from numerics, line segments join them to guide the eye. The threshold from (49) is $\eta = 10\%$. Panel (b): data from the upper panel shown on a double logarithmic plot. The solid red line has the slope equal to +2 and the intercept fitted to the two largest- τ_Q data points.

	a	b
$20 \leq N \leq 30$	1.75(1)	-2.60(4)
$38 \leq N \leq 62$	1.871(3)	-3.03(1)
$70 \leq N \leq 142$	1.92(1)	-3.26(6)
$200 \leq N \leq 300$	1.970(4)	-3.48(2)

TABLE VI: The results of fitting (51) to numerical data in different ranges of the system sizes (either four or five data points are used for each linear regression). We provide one standard error in the brackets delivered by the `LinearModelFit` function from [33].

at the vanishing magnetic field. They bring the system to the desired value of this field, where the symmetry-breaking gap can be read from the subsequent free-evolution dynamics of the longitudinal magnetization. In this way a small symmetry-breaking gap can be seen through large-amplitude oscillations of the longitudinal magnetization.

We have discussed different ways of analyzing the oscillatory dynamics of such magnetization showing that one can also extract the equilibrium longitudinal magnetization out of them. All this can be accurately done if the quench is slow enough, which we have studied in the context of the Kibble-Zurek theory of non-equilibrium phase transitions. An excellent agreement between predictions of this theory and the dynamics of the longitudinal magnetization has been found.

Although our studies have been done in the Ising model, they can be extended to other systems exhibiting the symmetry-breaking phenomenon. For example, the Ising-like ones with long-range interactions that are typically found in cold ion and atom emulators of spin systems [4, 5, 34, 38]. These systems provide a promising platform for experimental realization of the studies discussed in our work for two reasons. First, their size is finite rather than thermodynamic, which makes their symmetry-breaking gap large-enough to be experimentally measurable. This should not be taken for granted because it is not the case in traditional condensed matter setups used for the studies of phase transitions, where the samples' size is thermodynamic (see e.g. [39] for the relevant example). Second, there has been substantial progress in the experimental control of such systems, which has been recently demonstrated for several tens of such effective spins [36, 37, 40].

Talking about experimental realizations, the symmetry-breaking phenomenon was recently experimentally investigated in [6]. These studies were done in a cold atom cloud, where each atom was simulating the 16-spin Lipkin-Meshkov-Glick model. This is the Ising-like model with the nearest-neighbor spin-spin interactions replaced with identical couplings between all the spins. Besides exploration of a different Hamiltonian, these interesting studies differ from our work in the following aspects. First, the quenches start in the paramagnetic phase. Second, the initial state for them occupies one of the parity subspaces and so the symmetry-breaking perturbation is used to populate the other one as well. Third, perhaps most importantly, they are limited to one, rather small system size, and they do not explore the non-adiabatic Kibble-Zurek dynamics of the symmetry-breaking phenomenon, which is of key importance in our work.

Finally, we mention that we hope that this work will trigger interest in the experimental studies of the symmetry-breaking gap, which could lead to quantitative insights into the very nature of quantum phase transitions. This would be most interesting in systems that can be neither analytically nor numerically studied in the foreseeable future.

Acknowledgments

We thank Marek Rams for useful discussions, sharing with us the results of his numerical simulations, and reading the manuscript. MB and BD were supported by the Polish National Science Centre (NCN) grant DEC-2016/23/B/ST3/01152.

Appendix A: Diagonalization and time-evolution of open Ising chain

We will briefly summarize here technicalities related to diagonalization of the open Ising chain, computation of its longitudinal magnetization, and its time evolution.

Diagonalization. We follow here [41] providing an early take on this subject. The diagonalization begins with Jordan-Wigner spin-to-fermion mapping (28) transforming Hamiltonian (42) to the following quadratic form

$$\begin{aligned} \tilde{H} &= \Psi^\dagger \mathcal{H} \Psi, \\ \Psi^\dagger &= (c_1^\dagger \dots c_N^\dagger \ c_1 \dots c_N), \\ \mathcal{H} &= \begin{pmatrix} A & B \\ -B & -A \end{pmatrix}, \end{aligned} \tag{A1}$$

where A and B are $N \times N$ tridiagonal matrices

$$\begin{aligned} A_{ij} &= g \delta_{i,j} - 1/2 \delta_{i,j+1} - 1/2 \delta_{i+1,j}, \\ B_{ij} &= 1/2 \delta_{i,j+1} - 1/2 \delta_{i+1,j}. \end{aligned} \tag{A2}$$

We mention in passing that we have corrected a misprint from [41] in the expression for B_{ij} .

Next, for every value of the magnetic field g , one can perform the Bogolubov transformation

$$\begin{aligned} \Psi &= \beta \Gamma, \\ \Gamma^\dagger &= (\gamma_1^\dagger \dots \gamma_N^\dagger \ \gamma_1 \dots \gamma_N) \end{aligned} \tag{A3}$$

choosing real orthogonal matrix β in such a way that (A1) is diagonal. This leads to (43).

Finally, we mention that the symmetry-breaking gap can be analytically calculated at the critical point with results from [42]

$$\delta(g=1) = 4 \sin \frac{\pi}{4N+2} \approx \frac{\pi}{N}. \quad (\text{A4})$$

This is about twice larger than the symmetry-breaking gap in the periodic chain (11).

Equilibrium longitudinal magnetization. To compute the equilibrium longitudinal magnetization M_x^{eq} we evaluate (45) in the state

$$\frac{|GS\rangle + \gamma_1^\dagger|GS\rangle}{\sqrt{2}}, \quad (\text{A5})$$

where $|GS\rangle$ is the ground state annihilated by all γ_i operators. This leads to the following expression for the longitudinal magnetization after employment of Wick's theorem

$$M_x^{eq} = \langle GS| \gamma_1 \sigma_{N/2}^x |GS\rangle. \quad (\text{A6})$$

The operator $\gamma_1 \sigma_{N/2}^x$ can be conveniently written as

$$\gamma_1 \sigma_{N/2}^x = \gamma_1 a_{N/2} b_{N/2-1} a_{N/2-1} \dots b_1 a_1, \quad a_i = c_i + c_i^\dagger, \quad b_i = i(c_i^\dagger - c_i). \quad (\text{A7})$$

Using Wick's theorem again, one can show that

$$\langle GS| \gamma_1 \sigma_{N/2}^x |GS\rangle = \text{Pf}(G),$$

$$G = \begin{pmatrix} 0 & \langle \gamma_1 a_{N/2} \rangle & \langle \gamma_1 b_{N/2-1} \rangle & \langle \gamma_1 a_{N/2-1} \rangle & \dots & \langle \gamma_1 a_1 \rangle \\ & 0 & \langle a_{N/2} b_{N/2-1} \rangle & \langle a_{N/2} a_{N/2-1} \rangle & \dots & \langle a_{N/2} a_1 \rangle \\ & & 0 & \langle b_{N/2-1} a_{N/2-1} \rangle & \dots & \langle b_{N/2-1} a_1 \rangle \\ & & & & \vdots & \\ & & & & & 0 \end{pmatrix}, \quad (\text{A8})$$

where Pf stands for Pfaffian, the lower triangle of the G matrix can be obtained by the relation $G = -G^T$, and the expectation values are calculated in the ground state $|GS\rangle$. Pfaffians of skew-symmetric matrices can be efficiently computed using Hausholder transformation [43].

Time-evolution. We work in the Heisenberg picture. Our evolutions start at time t_0 from the equal superposition of the two lowest-energy eigenstates of $\tilde{H}[g(t_0)]$

$$\frac{|GS[g(t_0)]\rangle + \gamma_1^\dagger|GS[g(t_0)]\rangle}{\sqrt{2}}. \quad (\text{A9})$$

Using quench protocol (4), one gets $g(t_0) = -g_f \tau_Q = 0$. It is numerically convenient for us, however, to begin evolutions from the slightly non-zero g , which we do by choosing t_0 such that $g(t_0) = 10^{-3}$.

Time-dependent longitudinal magnetization (45) is then expressed as

$$M_x(t) = \text{Re} \langle GS[g(t_0)] | \gamma_1 \sigma_{N/2}^x(t) | GS[g(t_0)] \rangle, \quad (\text{A10})$$

where the operator γ_1 is defined at time t_0 . The matrix element in this equation can be computed just as (A8) expect a_i and b_i operators are now time dependent. Thus, we need to know their time evolution, which can be extracted from

$$\Psi(t) = U(t)\Psi(t_0), \quad (\text{A11})$$

where the $N \times N$ unitary matrix $U(t)$ can be obtained by solving

$$\frac{d}{dt}U(t) = -2i\mathcal{H}U(t) \quad (\text{A12})$$

with the initial condition $U(t_0) = \mathbb{1}$. Equation (A12) can be derived from the Heisenberg equations for the $c_i(t)$ and $c_i^\dagger(t)$ operators. We solve it numerically with the Suzuki-Trotter method of order two [44].

Having $U(t)$ and the Bogolubov matrix β at the time t_0 , we can relate $c_i(t)$ and $c_i^\dagger(t)$ operators to γ_i and γ_i^\dagger appearing in the diagonal form of $\tilde{H}[g(t_0)]$. Namely,

$$\Psi(t) = W(t)\Gamma, \quad W(t) = U(t)\beta, \quad (\text{A13})$$

where the matrix W has the following structure

$$W = \begin{pmatrix} C & D \\ \overline{D} & \overline{C} \end{pmatrix} \quad (\text{A14})$$

with C and D being $N \times N$ complex matrices. Transformation (A13) can be used to compute all correlation functions, from time-dependent version of (A8), needed for getting (A10). For example, after straightforward manipulations one can show that

$$\langle a_i a_j \rangle = \sum_{k=1}^N (C_{ik}D_{jk} + C_{ik}\overline{C_{jk}} + D_{ik}\overline{D_{jk}} + \overline{D_{ik}}\overline{C_{jk}}). \quad (\text{A15})$$

- [1] S. Sachdev *Quantum Phase Transitions* (Cambridge University Press, 2011).
- [2] M. Continentino *Quantum Scaling in Many-Body Systems: An Approach to Quantum Phase Transitions* (Cambridge University Press, 2nd edition, 2017).
- [3] S. Sachdev and B. Keimer, Phys. Today **64**, 29 (2011).
- [4] M. Lewenstein, A. Sanpera, V. Ahufinger, B. Damski, A. Sen De, and U. Sen, Adv. Phys. **56**, 243 (2007).
- [5] C. Gross and I. Bloch, Science **357**, 995 (2017).
- [6] V. Makhalov, T. Satoor, A. Evrard, T. Chalopin, R. Lopes, and S. Nascimbene, arXiv:1905.00807 (2019).
- [7] E. Lieb, T. Schultz, and D. Mattis, Ann. Phys. (N.Y.) **16**, 407 (1961).
- [8] J. Dziarmaga, Phys. Rev. Lett. **95**, 245701 (2005).
- [9] W. H. Zurek, U. Dorner, and P. Zoller, Phys. Rev. Lett. **95**, 105701 (2005).
- [10] A. Polkovnikov, Phys. Rev. B **72**, 161201(R) (2005).
- [11] S. Mostame, G. Schaller, and R. Schützhold, Phys. Rev. A **76**, 030304(R) (2007).
- [12] R. Barankov and A. Polkovnikov, Phys. Rev. Lett. **101**, 076801 (2008).
- [13] S. Mondal, K. Sengupta, and D. Sen, Phys. Rev. B **79**, 045128 (2009).
- [14] D. Patanè, L. Amico, A. Silva, R. Fazio, and G. E. Santoro, Phys. Rev. B **80**, 024302 (2009).
- [15] L. Cincio, J. Dziarmaga, M. M. Rams, and W. H. Zurek, Phys. Rev. A **75**, 052321 (2007).
- [16] K. Sengupta and D. Sen, Phys. Rev. A **80**, 032304 (2009).
- [17] A. Das, Phys. Rev. B **82**, 172402 (2010).
- [18] M. Kolodrubetz, B. K. Clark, and D. A. Huse, Phys. Rev. Lett. **109**, 015701 (2012).
- [19] A. Francuz, J. Dziarmaga, B. Gardas, and W. H. Zurek, Phys. Rev. B **93**, 075134 (2016).
- [20] A. Russomanno, S. Sharma, A. Dutta, and G. E. Santoro, J. Stat. Mech. (2015) P08030.
- [21] T. Puskarov and D. Schuricht, SciPost Phys. **1**, 003 (2016).
- [22] S. Lorenzo, J. Marino, F. Plastina, G. M. Palma, and T. J. G. Apollaro, Sci. Rep. **7**, 5672 (2017).
- [23] M. Białończyk and B. Damski, J. Stat. Mech. (2018) 073105.

- [24] M. M. Rams, J. Dziarmaga, and W. H. Zurek, Phys. Rev. Lett. **123**, 130603 (2019).
- [25] P. Pfeuty, Ann. Phys. **57**, 79 (1970).
- [26] B. Damski and M. M. Rams, J. Phys. A **47**, 025303 (2014).
- [27] B. Damski, Phys. Rev. Lett. **95**, 035701 (2005).
- [28] T. W. B. Kibble, Phys. Rep. **67**, 183 (1980).
- [29] W. H. Zurek, Phys. Rep. **276**, 177 (1996).
- [30] A. del Campo, T. W. B. Kibble, and W. H. Zurek, J. Phys.: Condens. Matter **25**, 404210 (2013).
- [31] A. del Campo and W. H. Zurek, Int. J. Mod. Phys. A **29**, 1430018 (2014).
- [32] J. Dziarmaga, Adv. Phys. **59**, 1063 (2010).
- [33] Wolfram Research, Inc., Mathematica, Version 11.0, Champaign, IL (2016).
- [34] S. Korenblit *et al.*, New J. Phys. **14** 095024 (2012).
- [35] O. A. Prośniak, Phys. Scr. **94**, 085201 (2019).
- [36] H. Bernien *et al.*, Nature **551**, 579 (2017).
- [37] J. Zhang, G. Pagano, P. W. Hess, A. Kyprianidis, P. Becker, H. Kaplan, A. V. Gorshkov, Z.-X. Gong, and C. Monroe, Nature **551**, 601 (2017).
- [38] D. Porras and J. I. Cirac, Phys. Rev. Lett. **92**, 207901 (2004).
- [39] R. Coldea, D. A. Tennant, E. M. Wheeler, E. Wawrzynska, D. Prabhakaran, M. Telling, K. Habicht, P. Smeibidl, and K. Kiefer, Science **327**, 177 (2010).
- [40] A. Keesling *et al.*, Nature **568**, 207 (2019).
- [41] A. P. Young, Phys. Rev. B **56**, 11691 (1997).
- [42] G. G. Cabrera and R. Jullien, Phys. Rev. B **35**, 7062 (1987).
- [43] M. Wimmer, ACM Trans. Math. Software **38**, 30 (2012).
- [44] N. Hatano, M. Suzuki, Eds. A. Das and B.K. Chakrabarti (Springer, Berlin, 2005) pp. 37-68.